AD

STRESS CONCENTRATORS AND RATE EFFECTS IN FORMATION OF ADIABATIC SHEAR BANDS

Final Technical Report

(End of the second year 1996/1998)

by Janusz R. Klepaczko

January 1998

UNITED STATES ARMY

EUROPEAN RESEARCH OFFICE OF THE US ARMY

LONDON, ENGLAND

CONTRACT N° N68171-97-C-9003

Contractor:

Laboratoire de Physique et Mécanique des Matériaux
UMR CNRS 7554
Institut Supérieur de Génie Mécanique et Productique
UNIVERSITE DE METZ
F-57045 Metz, France

Approved for Public Release
Distribution Unlimited

AD

STRESS CONCENTRATORS AND RATE EFFECTS IN FORMATION OF ADIABATIC SHEAR BANDS

Final Technical Report

(End of the second year 1996/1998)

by Janusz R. Klepaczko

January 1998

UNITED STATES ARMY
EUROPEAN RESEARCH OFFICE OF THE US ARMY
LONDON, ENGLAND

CONTRACT N° N68171-97-C-9003

Contractor:

Laboratoire de Physique et Mécanique des Matériaux
UMR CNRS 7554
Institut Supérieur de Génie Mécanique et Productique
UNIVERSITE DE METZ
F-57045 Metz, France

REPORT DOCUMENTATION PAGE

Form Approved
OMB No. 0704-0188

1. AGENCY USE ONLY (Leave Blank)	2. REPORT DATE	3. REPORT TYPE AND DATES COVERED

4. TITLE AND SUBTITLE
STRESS CONCENTRATORS AND RATE EFFECTS IN FORMATION OF ADIABATIC SHEAR BANDS

5. FUNDING NUMBERS
CONTRACT N°N68171-97-C-9003
PROJECT N°WK2Q6C-8117-AN01

6. AUTHOR(S)
J.R. KLEPACZKO

7. PERFORMING ORGANIZATION NAME(S) AND ADDRESS(ES)
METZ UNIVERSITY - I.S.G.M.P.
LAB. OF PHYSICS & MECHANICS OF MATERIALS
ILE DU SAULCY F-57045 METZ, FRANCE

8. PERFORMING ORGANIZATION REPORT NUMBER
N/A

9. SPONSORING/MONITORING AGENCY NAME(S) AND ADDRESS(ES)
USARDSG-UK, AERONAUTICS AND MECHANICS BRANCH
Dr R. REICHENBACH, EDISON HOUSE
223 OLD MARYLEBONE RD, LONDON NW1-5TH UK

10. SPONSORING /MONITORING AGENCY REPORT NUMBER

11. SUPPLEMENTARY NOTES
List of published papers

12a. DISTRIBUTION/AVAILABILITY STATEMENT
DISTRIBUTION UNLIMITED

12b. DISTRIBUTION CODE
N/A

13. ABSTRACT (Maximum 200 words)

This Final Technical Report covers the contract period from Nov. 7/1996 to Jan. 6/1998. A more detailed information on the progress of this Contract can be found in the previous Interim Reports. During the period under consideration the research has been continued on analyses of experimental results obtained via the Modified Double Shear experimental technique (MDS). This technique has been applied for VAR 4340 steel with the heat treatment to ~50 HRC. In order to study the effect of stress concentrators in shear at different rates of loading four MDS geometries have been tested with different stress concentrators, from « standard » geometry to a very sharp notch. A wide loading rate spectrum has been covered, from quasi-static to impact (up to impact velocity ~100 m/s). Experiments confirmed that the adiabatic stress concentrators accelerate failure in shear. This mechanism leads to a decrease of the fragmentation energy when the impact velocity is increased. In parallel, the numerical studies for all four geometries have been performed using the FE code ABAQUS. Details of the numerical studies are given in the Appendix to this Report. The numerical analyses have confirmed all observations from experiments.

14. SUBJECT ITEMS
ADIABATIC SHEAR BANDS, STRESS CONCENTRATORS IN IMPACT FAILURE
DYNAMIC PLASTICITY

15. NUMBER OF PAGES
1

16. PRICE CODE

17. SECURITY CLASSIFICATION OF REPORT	18. SECURITY CLASSIFICATION OF THIS PAGE	19. SECURITY CLASSIFICATION OF ABSTRACT	20. LIMITATION OF ABSTRACT
UNCLASSIFIED	UNCLASSIFIED	UNCLASSIFIED	

NSN 7540-01-280-5500

Standard Form 298 (Rev. 2-89)
Prescribed by ANSI Std. Z39-18
298-102

CONTENTS

EXTENDED ABSTRACT

This Extended Abstract covers the activities on the « Stress Concentrator and Rate Effect in Formation of Adiabatic Shear Bands » carried out during two years (Contract N° N68171-95-C-9071 and Contract N° N68171-97-C-9003). The Report covers the period from Nov. 7/1996 to Jan. 6/1998. During this period an investigation was conducted into the effect of the adiabatic stress concentrators on development of the adiabatic shear bands (ASB) and failure in the shear mode. The effects of the imposed velocities, including impact up to 120 m/s, on the ASB's formation and failure have been studied for VAR 4340 steel, ~50 HRC. In parallel to experiments an extended numerical studies have been performed, up to impact velocities 180 m/s.

Experiments on impact shearing have been performed on four specimen geometries with different stress concentrators, from a more uniform stress field (standard geometry) to a sharp notch. Each geometry was tested within a wide range of velocities, from $2 \cdot 10^{-6}$ m/s to 120 m/s, increased by 19 steps. At higher velocities, from 10 m/s to 120 m/s, a direct impact technique of a projectile on the Modified Double Shear (MDS) specimen have been applied.

For all four geometries and for all imposed velocities the results have been obtained in the form of the nominal shear stress τ_n versus the nominal shear strain Γ_n. The characteristic points of those curves like the instability strain Γ_{nc} and the final localization strain Γ_{nl} at failure have been found. At velocities higher than ~0.02 m/s a substantial drop of the instability strain was observed. This leads to a substantial drop of the failure energy when the impact velocity is increased. The adiabatic stress concentrators facilitate the failure in the shear mode.

In order to assure a well defined input into the numerical studies a new form of the constitutive relation has been derived. The constitutive relation, completely coupled with temperature, is based to some extent on the material science approach.

In parallel, an extensive numerical study have been completed on wave effects and adiabatic stress concentrators. The explicit FE code ABAQUS was used in this study. It has been found during the first series of calculations that the plastic work produces an increase of the local temperature around a stress concentrator which in turn accelerates failure due to thermal softening. Around the notch tips a zone of large plastic deformation and high temperature are formed very rapidly. The numerical study confirmed existence of the Critical Impact Velocity in shear (CIV). It has been found that the trapping of plastic shear waves by adiabatic instability is the main cause of the CIV in shear. The CIV can be precisely estimated by the FE technique. A good correlation was found for VAR 4340 steel between the CIV found by FE code and experiment.

During the last year of the Project an introduction of a local failure criterion in the FE code was studied. The following two local criteria were tested : a) the local maximum inelastic deformation in the adiabatic conditions ; b) the local maximum value of the adiabatic strain energy density. Both criteria permit for numerical analyses of the fragmentation processes. A general conclusion can be drawn that in the case of impact shearing the failure is more sensitive to the adiabatic stress concentrators at higher impact velocities. Complete results of the FE study are given in Appendix N°1 to this Report.

List of Keywords : Adiabatic shear bands
High strength steels
VAR 4340 steel
Shear test
Shear failure
Dynamic plasticity

1. Objectives of the Project and general remarks

Previous studies which were carried out under support of the ERO-London have shown that the formation of the adiabatic shear bands (ASB) in metals is sensitive to the velocity of shearing [1, 2, 3]. This is caused by variety of effects like strain hardening, strain rate and temperature sensitivity of the flow stress and inertia. Since the imposed velocity of shearing can be changed from very low to low–velocity impact (~100 m/s) and further to the ballistic velocities (~1000 m/s), expected reaction of a material may substantially differ. Preliminary numerical calculations by the finite difference technique of the adiabatic shear localization have shown that for a perfect layer in the steady state of shear (no stress concentrators) the rate sensitivity and inertia delay the process of localization, Stages 2 and 3, [4]. On the contrary, experiments performed in the configuration of impact shearing clearly demonstrated that the shear localization is accelerated when the imposed velocity is increased. This apparent contradiction was the main reason to continue this study on different impact velocities and stress concentrators in adiabatic shearing. It has appeared that the stress concentrators play a very important role in adiabatic instabilities and adiabatic failure of metallic materials. In order to gain more information on the effect of stress concentrators triggered in dynamic conditions (impact) and rate effects in formation of the ASB's, experimental studies have been undertaken. Different stress concentrators have been studied in shear for VAR 4340 steel, ~50 HRC.

On the other hand numerical calculations by FE explicit code ABAQUS with more realistic initial and boundary conditions have been performed [5, 6]. It was intended to verify available experimental results obtained in LPMM-Metz for VAR 4340 steel (~50 HRC). The experimental technique of direct impact on the MDS specimen was used during testing of this steel, [1, 7, 8]. The experimental finding was confirmed by the FE calculations that the Critical Impact Velocity in shear (CIV) is a kind of a new material constant.

All numerical calculations for VAR 4340 steel have been performed with a specially developed constitutive relations based in part on material science.

In order to understand more the role of the adiabatic stress concentrators in shear failure under impact, four geometries of the specimen with different stress concentrators were assumed. The most acute stress concentrator was produced by the spark erosion technique.

The numerical analyses were continued with the FE explicit code ABAQUS along with the local failure criteria.

This approach permitted to study further the effect of the adiabatic stress concentrators activated at different loading rates on failure. Two independent failure criteria were introduced in the FE code. The main objective to resolve the discrepancy between experimental results (existence of the stress concentrators) and previous numerical result seems to be accomplished.

2. Experimental technique and Modified Double Shear (MDS) geometry

This experimental technique, which has been described in details in [1, 7, 8], is operational since 1991 in LPMM-Metz. Because the test theory and details of this technique is given elsewhere, [7], here only a brief description is offered. Fig. 1 shows the operational principles. Because of flexibility of specimen attachment to the loading device (a hydraulic machine or Hopkinson tube) different geometries of the shear zone can be applied.

The MDS specimen with its new standard geometry, which prevents plastic deformation and rotation of the supports, has been discussed in [7]. The deformed layer of the MDS specimen has 2 mm and it initially assures the uniform deformation over the gage length at low nominal strain rates. The MDS specimens are loaded by direct impact using a bar projectile, as it is shown in Fig. 1. The scheme of loading by direct impact permits for greater flexibility in programming of the nominal strain rate in shear, simply by changing the impact velocity. The rise-time with this type of loading is very short in comparison, for example, to SHTB technique. The flat-ended projectiles of different lengths and diameter d_p=10 mm, are launched from an air gun with predetermined velocities V_i, 1 m/s $\leq V_i \leq$ 200 m/s. The impact velocity V_i is measured by three sources of light 1, fiber optics 3, three independent photodiodes 2 and two time counters 4. Axial displacement $\delta_X(t)$ of the central part of the MDS specimen is measured as a function of time by an optical, non-contact, displacement transducer 8. The optical transducer reacts to the axial movements of a small black and white target cemented to the central part of the MDS specimen, channel 1. Since the impact end of the projectile is black, the displacement of the contact between the projectile and MDS specimen is measured in the same way, channel 2.

The axial force transmitted by the specimen symmetric supports can be determined as a function of time from the transmitted longitudinal elastic waves $\varepsilon_T(t)$ measured by strain gages 7, DC supply units 11 and amplifier 10. All electric signals, that is voltages of displacement $V_X(t)$ and $V_C(t)$ and transmitted wave $\varepsilon_T(t)$ are recorded by a digital osciloscope 12 and stored later in the computer hard disc 13 for further analyses. After analyses of the recorded signals and elimination of time, a force-displacement curve can be constructed for the MDS specimen and $\tau(\Gamma)$ and $\dot{\Gamma}(\Gamma)$ finally determined, where τ and Γ are respectively the shear stress and shear strain, t is time and $\dot{\Gamma} = d\Gamma / dt$.

The experimental technique based on the MDS specimen and direct impact has appeared to be quite effective for materials testing at high strain rates in shear, 10^3 $s^{-1} \leq \dot{\Gamma} \leq 10^5$ s^{-1}. Typical oscillogram of such test is shown in Fig. 2. The MDS specimen made of VAR 4340 steel, ~52 HRC (standard geometry) was loaded by projectile L_p=200 mm at impact velocity V_i=72.3 m/s. The two channel digital oscilloscope with the sampling rate 1 GHz was triggered by the signal from the optical transducer, channel 1. It is visible that the velocity of the central part of the MDS specimen is almost constant, no vibrations are present. The theoretical time of contact is $t_c=2L_p/C_o$ where C_o is the elastic wave speed in

bar, $C_o \approx 5.0$ mm/μs, finally $t_c = 80$ μs, the time interval much longer in comparison to the rupture time of this specimen, $t_f \cong 14$ μs. The transmitted wave is recorded by channel 2. The delay to propagate the elastic longitudinal wave in the Hopkinson tube, from the specimen to the strain gage is $t_d \cong 37.2$ μs. A special computer program has been developed to analyse the oscillograms and to determine $\tau(\Gamma)$ and $\dot{\Gamma}(\Gamma)$ curves.

3. Effect of impact velocity on MDS specimen, the Critical Impact Velocity in shear

It has been shown recently, [9] and [10], that during shear deformation imposed by a high-velocity impact plastic waves exited in a deformed material can completely change the mechanics of plastic field. As a rule, an intense plastic deformation will appear near the impact end of a specimen. In the case of the MDS specimen with the gage length 2.0 mm the nominal strain rate when the plastic waves start to dominate is $5 \cdot 10^4$ 1/s, that is the velocity of shearing is ~100 m/s.

Since formulation of the rate independent theory of elasto-plastic waves in solids by Karman, Taylor and Rakhmatulin in late forties and early fifties, for a review see [11], it is known that the longitudinal plastic deformation can be localised in thin bars by a high velocity impact, [12]. This deformation trapping by longitudinal plastic waves is called Critical Impact Velocity in tension, [12] and [13].

It has been shown recently that the Critical Impact Velocity in shear can be determined experimentally using the MDS specimen and the direct impact loading, [9] and [10]. An existence of the CIV in shear was predicted by FE numerical method in [14]. A more detailed analytic study was published elsewhere, [10], here only a brief discussion is offered.

It is clear that the CIV in shear is closely related with adiabatic heating and thermal softening. The CIV in shear is caused by an instantaneous instability and strain localization superimposed on plastic wave propagation in shear. The rate-independent wave propagation theory has been applied to analyse the CIV in shear and the final formula was derived in [10].

Preliminary numerical calculations of the CIV for 1018 steel (French Standard XC18) have confirmed the usefulness of the analytic procedure presented in [10]. The value of CIV obtained with a simplified constitutive relation was $V_{cr} = 98$ m/s and $\dot{\Gamma}_c = 4.9 \cdot 10^4$ 1/s for 2.0 mm gage length, the value very close to the one determined by the MDS specimen and direct impact technique, $V_{cr} \cong 90$ m/s. The experimental technique based on the MDS specimen and direct impact has been applied so far for the determination of the CIV for VAR 4340 (52 HRC), the value found was ≅140 m/s, [10].

In order to study further the CIV phenomenon, a numerical study of impact shearing of a layer has been performed by the FE code ABAQUS. It was intended to verify available experimental results for VAR 4340 steel, ~50 HRC, obtained by direct impact on the MDS

specimen, [1]. In particular, the numerical study has been focused on the effect of the impact velocity including the phenomenon of the Critical Impact Velocity in shear. An infinite thin layer fixed at one end and with a small geometrical imperfection in the middle of its height was considered. The layer was submitted in the other end to different shear velocities, from quasi-static to impact, up to 180 m/s. All details of those calculations are given elsewhere, [5, 6], the final results are shown in Fig. 3, [15].

Two modes of shear deformation of the layer have been found: in the first mode all deformations concentrates in the middle of the layer, and in the second near the surface where the shear velocity was imposed. The CIV could be defined as a transition between those two modes. It has been shown that impact velocities higher than the CIV lead to a substantial reduction of the localization energy, Fig. 4.

All FE calculations have been performed with constitutive relations specially developed to reflect behavior of VAR 4340 steel. Thermal coupling, strain hardening and rate sensitivity were accounted for. Introduction of the temperature-dependent strain hardening exponent has demonstrated the importance of the proper formulation of the constitutive relations for all thermal instability problems. The constitutive relations are discussed later on in this Report.

Overall good correlation with experimental results and physical intuition have been achieved.

4. Constitutive relations

In the FE codes available on the market the constitutive relations are usually quite simple and not specifically tailored to particular problems. All problems of plastic instabilities including thermal coupling must be analysed with a precise and reliable constitutive relation or relations. Precision of the model reflects later the FE results. In order to approximate adiabatic instabilities, localization and wave effects, constitutive relations must include strain hardening, rate sensitivity and temperature sensitivity of the flow stress within a wide range of strains, strain rates and temperatures. After careful analyses of experimental data available in open literature for VAR 4340 steel, ~50 HRC, the following explicit form of the constitutive relation has been worked out

$$\tau = \frac{\mu(T)}{\mu_o}\left[B\left(\frac{T}{T_o}\right)^{-\nu}\left(\Gamma_o + \Gamma\right)^n + \tau_o\left(1 - \frac{T}{D}\log\frac{\dot{\Gamma}_o}{\dot{\Gamma}}\right)^m\right] \tag{1}$$

where B, μ_o, υ, n, m are respectively, the modulus of plasticity, the shear modulus at T=300 K, the temperature index, the strain hardening exponent and the logarithmic rate sensitivity, T_o, Γ_o and $\dot{\Gamma}_o$ are normalization constants. The temperature change of the shear modulus is given by

$$\mu(T) = \mu_o[1-AT^*-CT^{*2}]; \quad T^* = T - T_{RT} \quad T_{RT} = 300K \tag{2}$$

where A and C are constants, and $T^* = T - T_{RT}$ is the modified temperature. In principle, this version of constitutive equations can be applied at RT and temperatures higher than 300 K.

At the beginning a simplified version of the constitutive relation (1) was used in the preliminary FE calculations. In this approach the strain hardening exponent n was assumed as constant. It appeared that the process of localization is unrealistically extended into large strains because of a strong parabolic hardening. It is known, however, that the rate of strain hardening in steel is temperature dependent and it diminishes with an increase of temperature, [16]. In the second approach n was assumed as a linearly decreasing function of the homologous temperature, [16]

$$n(T) = n_o(1-T/T_m) \tag{3}$$

where n_o is the strain hardening exponent at T=0 K and T_m is the melting point. This modification was found essential for VAR 4340 steel.

The structure of the constitutive relation has some elements based on the material science approach. First of all the level of stress is normalised by $\mu(T)/\mu_o$ which takes into account the thermal softening of the crystalline lattice. The first expression in the brackets is simply the internal stress and the second one is the rate and temperature-dependent effective stress, [17].

The procedure of how the constitutive relations have been developed is described with details in [5].

Total number of constants in eqs (1)-(3) is 12 and they are given in Table 1 and in Appendix N°1 to this Report.

Table 1. Material constants for VAR4340 steel, ~50 HRC

Const.	Value	Unit	Const.	Value	Unit
B	1493.0	MPa	A	$5.047 \cdot 10^{-4}$	1/K
μ_o	80769.0	MPa	C	$1.036 \cdot 10^{-7}$	$1/K^2$
υ	0.39	-	D	2914.0	K
n	eq. 3	-	τ_o	622.0	MPa
n_o	0.135	-	β	0.9	-
m	2.776	-	λ	38.0	W/mK
T_o	300.0	K	ρ	7890.0	kg/m^3
Γ_o	$1.6 \cdot 10^{-3}$	-	C_v	460.0	J/kgK
$\dot{\Gamma}_o$	10^6	1/s	T_m	1812.0	K

Majority of results of numerical simulations of the CIV in shear were obtained with the modified version of the constitutive relation n(T), however, some results with the constant value of n were also produced, mainly, in order to make comparison of the FE results where both relations are used. Complete FE results are reported elsewhere [5], in this Report only the most important results are discussed. It should be noted that modification of the constitutive relation by n(T) changes only certain temperature-dependent terms in eq. (3), for instance, both constitutive relations have identical strain rate sensitivity.

The most important part of the numerical analyses is the thermal coupling. The adiabatic increase of temperature can be estimated from eqs (1), (2) and (3). For this purpose, the flow stress τ is taken as a universal function of the shear strain Γ, the shear strain rate $\dot{\Gamma}$, and the temperature T, so that

$$\tau = \tau\left(\Gamma, \dot{\Gamma}, T\right) \tag{4}$$

It follows from energy conservation that

$$\frac{dT}{d\Gamma} = \frac{\left[1-\xi(\Gamma,T)\right]\tau\left(\Gamma,\dot{\Gamma},T\right)}{\rho_o(T)C_v(T)} \tag{5}$$

where $\xi(\Gamma,T)$ is a coefficient representing stored energy in the lattice, $\rho_o(T)$ is the density of the metal, and $C_v(T)$ is its specific heat at constant volume. The coefficient of stored energy on average is $\xi \approx 0.05$. Equation (5) can not be integrated in closed form unless certain simplifications are made. Since ρ_o is only weakly dependent on temperature it can be taken as a constant; at higher temperature than ~100 K, C_v may also be assumed as a constant. Furthermore, T can be set equal to the initial temperature T_o. Integration now becomes possible so long as one specifies $\dot{\Gamma}(\Gamma)$, that is, so long as one specifies changes in strain rate during the course of deformation. Thus an explicit form $\Delta T(\Gamma_m, T_o)$ is derived for the increase in temperature per unit volume during adiabatic deformation. With these simplifications, eq. (5) can be expressed as

$$\Delta T = \frac{1-\xi}{\rho_o(T_o)C_v(T_o)} \int_0^{\Gamma_m} \tau\left[\Gamma, \dot{\Gamma}(\Gamma), T_o\right] d\Gamma \tag{6}$$

Once $\Delta T\left(\Gamma_m, T_o\right)$ has been evaluated, then eq. (4) provides values of $\Delta\tau\left(\Gamma_m, T_o\right)$. Thus

$$\Delta\tau = \tau_T\left(\Gamma_m, \dot{\Gamma}, T_o\right) - \tau_A\left[\Gamma_m, \dot{\Gamma}, \left(T_o + \Delta T\right)\right] \tag{7}$$

where τ_T and τ_A are respectively the flow stress under isothermal and adiabatic conditions of deformation. Equation (7) can be used to compare adiabatic and isothermal stress-strain curves and to compare these curves with those of incremental rate experiments.

Thermal softening in shear due to the adiabatic heating leads to formation of an adiabatic shear band (ASB). The instability point defined as (τ_m, Γ_m) occurs at $\left(\partial\tau_A / \partial\Gamma\right) = 0$, Fig. 5. The instability point can be determined from equations (1), (2) and (3). It is important to note that the instability point in adiabatic shearing strongly depends on strain rate.

If the problem is complete, the FE calculations could be carried out with the thermal coupling. Since a large part of the plastic work is converted into heat the temperature of a material substantially increases when plastic deformation advances. The balance of energy with the heat conduction leads to the following relation

$$\beta\tau\frac{\partial\Gamma}{\partial t} = \rho C_v \frac{\partial T}{\partial t} - \lambda\frac{\partial^2 T}{\partial y^2} \tag{8}$$

where y is the axis of the heat conduction, β is the coefficient of energy conversion, $\beta=1-\xi$, and λ is the heat conductivity (Fourier constant). When the process is entirely adiabatic, $\lambda=0$, (no heat conduction) the heating is uniform in an elementary volume. All material constants are given in Table 1 and in Appendix N°1 to this Report.

The thermal characteristics which are discussed above permit for numerical simulations of all temperature-coupled problems as purely adiabatic as well as with the heat conduction. The code ABAQUS includes those thermal-coupling problems in the FE procedures.

5. Adiabatic stress concentrators

Crack initiation and fracture in metallic materials at various loading rates have been a subject of research for some time, for example [19]. Since the latest stage of ASB leads to fracture in Mode II, this Mode would dominate in all cases of impact shearing, including fragmentation and perforation. It is assumed in the theory of fracture mechanics that the crack tip has an infinitesimal radius and the stress concentrator is the most acute. If the loading rate of the small volume around the crack tip is relatively short this volume will be heated adiabatically and locally the adiabatic shear will be started. A more detailed analyses of the rate effects and stress fields at the crack tip in Mode II is given elsewhere [20, 21]. The main conclusion after those studies is that the boundaries of equal equivalent plastic strain at the crack tip in Mode II can be substantially reduced when the loading rate is increased. This leads to a more general conclusion: the stress concentrators behave in a more brittle manner at impact loading.

However, a stress concentrator may not be acute, in such case the plastic zone will be larger and the adiabatic heating will be more intense. A local failure criterion must be applied.

A specific case is the MDS geometry loaded with a relatively high shear velocity. Propagation of the elastic-plastic shear waves in such case is non-negligible. One example with a stress concentrator (V-type) is shown in Fig. 6. In this case the elastic-plastic shear wave (adiabatic) starts its propagation near the plane A-A. This wave is excited along x-axis by the shear velocity V_o, and it will propagate along y-axis with the wave speed $C_2(\Gamma)$, according to the rate-independent theory of wave propagation, [11]. The shear wave shown as the shadow region in Fig. 6 will approach the plane B-B with the stress concentrator, and next the tip of the stress concentrator will be deformed in the adiabatic conditions triggering severe plastic deformation. If the carrying capacity of the material will be reached a failure will appear. It will probably propagate along the maximum shear stress – one of possible criteria of failure. This simplified picture may explain, though, an interesting competition between two mechanisms of adiabatic failure. If the impact velocity V_o is high enough the shear wave can not be propagated into the notch direction and all plastic deformation will be concentrated near the surface A-A. This is so-called Critical Impact Velocity in shear (CIV), [5, 6, 8, 10, 14]. The CIV in shear is a specific mode of the adiabatic failure. If the impact velocity is slightly lower than the CIV two mechanism of failure will compete increasing the total failure energy within a narrow range of impact velocities.

Both mechanisms of failure are sensitive to the adiabatic stress concentrators and the impact velocity.

6. Experiments with different stress concentrators

The main interest to perform experiments with different stress concentrators was to study the effect of loading rate on formation of ASB's and adiabatic failure. The external geometry of the MDS specimens was kept unchanged and only the shearing zones have been modified.

Four geometries were applied as it is shown in Fig. 7, that is the standard geometry, Fig. 7a, the U-geometry, Fig. 7b, the V-geometry, fig. 7c, and the fine notch geometry, Fig. 7d. The ligament a as well as the thickness b were the same for all geometries, a=5.0 mm, b=6.0 mm with exception of the fine notch with a≈5.5 mm. Dimension of this notch, cut by the electro-sparking technique, was ~0.2 mm. The specimens were cut from the leftovers of the cross-rolled plate of VAR 4340 steel supplied earlier by the ARO-Watertown. After thermal treatment the Rockwell Hardness was ~50-52 HRC.

More details on the experimental technique, oscillogram analyses and the complete set of results are given in [15], the Report of the end of the first year.

In this Report only the mean values of the following characteristic points are shown and discussed. Namely, the maximum shear stress τ_m and the nominal shear strain Γ_m associated with τ_m, the critical stress τ_c where the fracture is detected after the force-displacement plot and associated critical strain Γ_c. Such situation is shown in Fig. 5, where the point (τ_m, Γ_m) is the instability point, the point (τ_c, Γ_c) is found normally in Stage 2 (quasi-brittle behavior), or during Stage 3 (advanced adiabatic shearing). As a rule $\tau_m \geq \tau_c$ and $\Gamma_m \geq \Gamma_c$. The nominal shear strain has been defined for the same way for ALL four geometries, $\Gamma_c=\delta(t)/h$, where $\delta(t)$ is the net displacement determined from the oscillograms as a function of time and h is the gage length in shear, h=2.0 mm.

The final results of those experiments are shown from Fig. 8 to Fig. 11 in the form of τ_m, τ_c, Γ_m and Γ_c as a function of the logarithm of the nominal strain rate $\dot{\Gamma}_n$ [s^{-1}]. In every figure are shown the mean values for four geometries studied. In the range of the small strain rates all four geometries show a positive rate sensitivity of the maximum stress τ_m. A similar behavior is found for the critical stress τ_c. It appears that the most "resistant" is the U-geometry, obviously with the most relaxed stress concentrator in comparison to the standard geometry. At higher strain rates the negative effect of adiabatic heating is obvious, the stress τ_m and τ_c decrease for all four geometries. Finally, at high nominal strain rates, $10^3\ s^{-1} \leq \dot{\Gamma}_n \leq 5 \cdot 10^4\ s^{-1}$ (2 m/s≤Vi≤100 m/s), values of τ_m increase, and τ_c is very close to τ_m which indicates a quasi-brittle behavior.

The mean values of the critical shear deformations differ substantially for different geometries, Figs 10 and 11. Again the largest deformations are observed for standard and U-geometries.

Because of reduced plasticity the rate sensitivity of shear stress is also reduced, which is visible in Fig. 8 and Fig. 9 for the standard geometry. The mean values of the rupture stress is from 600 MPa at low strain rates to 900 MPa at strain rate ~$5 \cdot 10^4\ s^{-1}$. The mean failure strain Γ_c increases within the region of smaller strain rates from ~0.018 at $\dot{\Gamma}=6 \cdot 10^{-4}\ s^{-1}$ up to $\Gamma_c \approx 0.03$ at $\dot{\Gamma}=1.0\ s^{-1}$, and next diminishes substantially to the level ~0.01 at $\dot{\Gamma}=10^4\ s^{-1}$. This effect is due to occurrence of adiabatic heating and formation of ASB's. It must be mentioned, however, that in overall the fracture behavior dominates at this level of hardness (50÷52 HRC). A similar behavior is found from the U-geometry, Figs 10 and 11. But the transition from isothermal to adiabatic regimes at $\dot{\Gamma}=1.0\ s^{-1}$ is more abrupt.

Geometries V and with sharp notch behave as almost brittle, and the transition from isothermal to adiabatic regimes are barely visible. The mean value of the maximum and failure stress is about 800 MPa for both cases. Reduced volumes of plastic zones around the notch tips reduce the nominal fracture deformation determined at low strain rates by LVTDs. In conclusion, at this level of hardness the level of brittleness obscures the typical behavior caused by thermally-coupled plasticity. It is well known that stress concentrators supress the volume of plastic zones.

The effect of stress concentrators and transition from isothermal to adiabatic regimes of failure is more distinct when the plastic energy to failure is analysed as a function of the logarithm of strain rate. Fig. 12 shows the plastic fracture energies respectively for the test series from standard to sharp notch geometry. Within the domain of small strain rates the energy increases at increasing strain rates, this is the case of standard and U-geometries. The maximum level is about 18 J to 19 J for the standard and U-geometries. The transition to the adiabatic regime is more abrupt for the U-geometry, and at high strain rates the plastic energy to fracture is almost zero. Such behavior is caused rather by stress concentrators and a local adiabatic instability, and not by, for example, the CIV in shear, usually observed for a more ductile metal. The stress concentrators trigger fracture-like processes at loading rates lower than the CIV in shear. Behavior of V- and sharp notch geometries is similar. At low strain rates the mean plastic energy to fracture is around 5 J for both geometries. At high strain rates the energies drop again to a very low level.

A general conclusion emerging after all series of tests on VAR 4340 steel (~50-52 HRC) with different stress concentrators is that at high loading rates this steel is much more prone to failure via adiabatic local failure than in the quasi-static conditions. Relatively high hardness reduces substantially plasticity and behavior is closer to fracture mechanics with a reduced process zone, for example [22].

The most important and practical conclusions on the role of the adiabatic stress concentrators in dynamic failure can be drawn from Fig. 12, where the mean failure energies are shown as a function of the logarithm of the nominal strain rate $\dot{\Gamma}_n$. The final results resemble closely the ductile to brittle transition observed via fracture mechanics tests or Charpy test. When an isolated crack or stress concentrator is loaded at increasing rates the total energy to fracture diminishes, [19]. The total energy to failure differs substantially for different stress concentrators. The highest resistance is found, as expected, for U-geometry and up to the medium strain rate, $\dot{\Gamma}_n \approx 1\ s^{-1}$, next an abrupt fall is observed from the level ~20 J to ~2 J at $\dot{\Gamma}_n \approx 30\ s^{-1}$, a drop of ten times. Behavior of the standard geometry, Fig. 7a, is similar, the sharper stress concentrators cause that the total energy of failure drops from ~13 J at $\dot{\Gamma}_n \approx 30\ s^{-1}$ to ~5 J at $\dot{\Gamma}_n \approx 100\ s^{-1}$.

The transition occurs $\sim 50\ s^{-1} \leq \dot{\Gamma}_n \leq \sim 110\ s^{-1}$, well below the CIV value which is around 120 m/s, Fig. 4, [1, 5]. Behavior of two geometries with the highest stress concentrators is similar. A drop of energy is still observed, however from the low constant level, ~5 J at $\sim 10^{-3}\ s^{-1} \leq \dot{\Gamma}_n \leq \sim 3.0\ s^{-1}$, to ~2 J above $\sim 10\ s^{-1}$.

In general, these experiments confirm that the adiabatic stress concentrators accelerate the failure processes failure at higher loading rates. In such case the impact velocity may be lower than the CIV in shear.

An evaluation of experimental findings by numerical methods is possible when a simple failure criterion is found.

7. Failure criteria in adiabatic shearing

Thermal softening during adiabatic heating leads directly to instability and localization and further on to failure in shear. In the case of pure adiabatic shear the condition for stability is reduced to the maximum shear stress $d\tau=0$. This condition can be rewritten into the form of zero tangent modules $d\tau/d\Gamma=0$ with the instability point (τ_m, Γ_m).

Application of the condition for stability $d\tau/d\Gamma=0$ and some form of equation for constitutive modeling leads to the final result in the form $\Gamma_m(\dot{\Gamma},T)$ when the adiabatic process of deformation is assumed together with a constant strain rate, [1, 9]. It has been found that an increase of flow stress when the strain rate is increased has a negative effect on the onset of adiabatic instability, that is Γ_m is reduced when strain rate is increased. The positive rate sensitivity increases production of plastic work converted into heat, this process accelerates formation of the instability, so values Γ_m are a diminishing function of the nominal strain rate. Several industrial steels tested so far in shear at strain rates from 10^{-3} to ~10^5 1/s with the MDS method, [7], showed a substantial evolution of the stress-strain curve. Schematic changes of the $\tau(\Gamma)$ curves observed for many industrial steels at increasing rates are shown in Fig. 13.

In this schematic figure the mean proportions are conserved to show the effect of the very high rate sensitivity on the yield stress and instability stress above ~10^3 1/s. On the contrary to the positive rate sensitivity of the critical stress τ_m, the critical strains of instability Γ_m always show a tendency to diminish when the strain rate is above ~10^3 1/s. The same happens with the failure strains. At very high strain rates such failure is even more abrupt, this occurs because of a superposition of the ASB development and plastic waves in shear.

In order to introduce a failure criterion into a numerical code it has been assumed that the failure starts at the instability point $\partial\tau/\partial\Gamma=0$ in the adiabatic conditions of deformation (high strain rates). Thus, it leads to the failure criterion based on the critical inelastic deformation $\Gamma_{pc}=\Gamma_m$. Of course, values of Γ_{pc} depend on strain rate and at a low strain rate (isothermal conditions) $\Gamma_{pc}\rightarrow\infty$. At high strain rates values of Γ_{pc} are substantially reduced according to the scheme shown in Fig. 13.

Since all material parameters in constitutive relations (1), (2) and (3) have been identified for VAR 4340 steel, values of $\Gamma_{pc}=\Gamma_m$ were found. The final result is shown in Fig. 14, where the calculated values of Γ_{pc} are shown as a function of $\log\dot{\Gamma}_n$. As a consequence of behavior shown in Fig. 13, values of Γ_{pc} decrease substantially up to strain rate ~10^4 1/s and then they stabilize.

In general case the failure $\Gamma_{pc}(\dot{\Gamma})$ criterion leads to formulation in the form of the equivalent plastic strain $\bar{\varepsilon}_p(\dot{\bar{\varepsilon}}_p)$ and equivalent plastic strain rate $\dot{\bar{\varepsilon}}_p$, thus

$$\bar{\varepsilon}_p = \frac{\sqrt{2}}{3}\left[(\varepsilon_{11}-\varepsilon_{22})^2+(\varepsilon_{22}-\varepsilon_{33})^2+(\varepsilon_{33}-\varepsilon_{11})^2+6(\varepsilon_{12}^2+\varepsilon_{23}^2+\varepsilon_{31}^2)^2\right]^{1/2} \tag{9}$$

with $\dot{\bar{\varepsilon}}_p = d\bar{\varepsilon}_p / dt$ (10)

when $\varepsilon_{12}\neq 0$ and $\varepsilon_{21}\neq 0$ and the remaining plastic strain components are zero, eqs (9) and (10) reduce to

$$\bar{\varepsilon}_p = \frac{2}{\sqrt{3}}\varepsilon_{12} \quad \text{and} \quad \dot{\bar{\varepsilon}}_p = \frac{2}{\sqrt{3}}\dot{\varepsilon}_{12} \tag{11}$$

$$\text{and} \quad \Gamma_p = 2\bar{\varepsilon}_p \,, \quad \dot{\Gamma}_p = 2\dot{\bar{\varepsilon}}_p \tag{12}$$

The failure criterion $\Gamma_{pc}(\log\dot{\Gamma})$ or $\bar{\varepsilon}_p(\log\dot{\bar{\varepsilon}}_p)$ can be easily introduced in any FE code. In fact, the code ABAQUS have already implemented such possibility.

Another failure criterion which can be derived using the situation shown in Fig. 13 is the criterion based on the « strain energy density » in the adiabatic conditions of deformation. Such criterion could be used for a large class of dynamic structural problems. The simplest failure criterion and most widely used in quasi-static metalworking processes has been proposed in [24],

$$C = \int_0^{\bar{\varepsilon}_f} \bar{\sigma}\, d\bar{\varepsilon} \tag{13}$$

where $\bar{\sigma}$ is equivalent stress

$$\bar{\sigma} = \frac{1}{\sqrt{2}}\left[(\sigma_{11}-\sigma_{22})^2+(\sigma_{22}-\sigma_{33})^2+(\sigma_{33}-\sigma_{11})^2+6(\sigma_{12}^2+\sigma_{23}^2+\sigma_{31}^2)^2\right]^{1/2} \tag{14}$$

$\bar{\varepsilon}_c$ is the critical equivalent strain, $\bar{\sigma}_c$ is the maximum equivalent tensile stress and $\bar{\varepsilon}$ is the total equivalent strain; the constant C is a material dependent critical value of strain energy per unit volume. This criterion indicates that failure occurs when the strain energy

per unit volume reaches a critical value. The critical value $\bar{\varepsilon}_c$ is usually assumed as a fracture strain obtained from tensile test either of a rod or a strip. Failure is then expected to occur at the position where the equivalent strain $\bar{\varepsilon}_c$ is reduced. In general, the « strain energy density criterion » is similar to the critical strain criterion. An energy density failure criterion was used for dynamic structural problems in [24] and also discussed in [25].

Since the adiabatic deformation dominates in the impact loading the failure criterion based on the « strain energy density » which takes into account the adiabatic instability has been specially developed during course of this study to be applied in computer codes. It is postulated that the adiabatic failure will occur when the total work reaches the critical value at $\bar{\varepsilon}_c$, where $\bar{\varepsilon}_c$ is the equivalent instability strain in adiabatic conditions of deformation. Again, constitutive relations (1)-(3) were used to calculate the energy at different strain rates

$$W_c = \int_0^{\Gamma_m} \tau(\Gamma)_A \, d\Gamma \; ; \quad \dot{\Gamma} = \text{const.} \tag{15}$$

where $\tau(\Gamma)_A$ is the adiabatic shear stress – shear strain relation, Fig. 5 and Fig. 13.

The final result in the form $W_c\left(\log\dot{\Gamma}\right)$ is shown is Fig. 14 as broken line. Of course, the critical value of the strain energy density diminishes as a function of strain rate up to shear strain rate ~10^3 1/s and next it stabilizes or even slightly increases. It is interesting to note that at high strain rates $10^2\ s^{-1} \le \dot{\Gamma} \le 10^5\ s^{-1}$ value of W_c obtained for VAR 4340 steel may be assumed constant, $W_c \approx 175$ MPa. Since both failure criteria give similar results, the further numerical studies were continued with the simplest criterion based on the critical equivalent strain in adiabatic conditions of deformation.

8. Numerical study of stress concentrators and adiabatic failure in impact shearing

An extended series of simulations have been carried out for all four geometries of shear layer with different stress concentrators, Fig. 7. The calculations have been performed for VAR 4340 steel using FE code ABAQUS/Explicit with constitutive relations (1)-(3) and failure criterion based on the ctitical values of deformation in adiabatic shearing. The Appendix to this Report contains complete results in the form of tabels and figures. Here, only the essential findings will be discussed.

In order to compare experimental results with numerical simulations several shear velocities were imposed, from 10 m/s to 150 m/s. Every simulation for each geometry and each imposed velocity V_i provided the following output functions:

(a) Failure patterns (paths of fracture) at different times and at different imposed velocities V_i;

(b) Temperature fields in shear layers at the instant of failure, including the hottest spots;

(c) Nominal shear strains at failure;

(d) Displacement δ_1 and δ_2 of the central part of Double Shear (DS) geometry for all DS geometries, δ_1 at the beginning of failure (elimination of the first element) and δ_2 – displacement at the complete failure (elimination of the last element);

(e) Reaction force R determined at the supports of each DS geometry for each imposed velocity V_i – analogy to the measured force in the MDS experiments;

(f) Determination of the mean stress τ via the reaction force R as a function of time; an analogy to experiment;

(g) The mean shear stress τ as a function of the nominal shear strain Γ_n for six different velocities V_i – from 10 m/s to 150 m/s;

(h) Energy of plastic deformation absorbed for each geometry as a function of the imposed velocity V_i.

This extended program of FE simulations appeared to be very helpful to understand better the mechanics of the MDS test and to demonstrate from the other hand application of the developed failure criterion.

For example, the failure patterns in the final stage of fracture for all four geometries (deformed configuration) are shown for three imposed velocities in figures from Fig. 15 to Fig. 18. The face B is from the support side.

From the fracture patterns shown for all four geometries in non-deformed configurations in Fig. 5 to Fig. 8 of the Appendix it is possible to estimate the mean propagation speed of the failure, that is elimination of the consequtive elements. It is interesting to note that the mean crack speed increases when the stress concentrator is sharper, standard geometry: $\dot{a} \approx 370$ m/s; U-geometry: ~400 m/s; V-geometry: ~690 m/s; Sharp notch geometry: ~1700 m/s.

An excellent demonstration of the transition of failure mechanism for the V-geometry is shown in Fig. 19, from the failure starter at the tip of the notch at lower impact velocities (50 m/s and 130 m/s) to the situation typical for the CIV in shear (impact velocities 160 m/s and 190 m/s). This is an analogy to discussion of Fig. 6 with the adiabatic stress concentrator. This is why superposition of plastic waves and stress concentrators give different failure patterns and different external reactions at different impact velocities. For

example, calculated maximum reaction force R_{max} for the DS supports are shown for all four geometries as a function of $\log(V_i)$ in Fig. 20 (also Fig. 15 in the Appendix). As expected, when the impact velocity exceeds 30 m/s the reactions differ for each geometry. For the standard and U-geometry the CIV in shear is well visible, but for the V-geometry value of the CIV is higher due to perturbation caused by the V-notch. The highest resistance to failure at high impact velocities is observed for the U-notch.

The results of calculations plotted in the form $\tau(\Gamma_n)$ determined by the analyses of the $R(\delta)$ characteristics, figures from Fig. 16 to Fig. 19 of the Appendix, show that the begining of failure seems to occur at relatively small nominal strains, for both low and high impact velocities. The end of fracturing at relatively low impact velocities occurs during descendant part of $\tau(\Gamma_n)$ curves, but at high velocities is closer to the maximum stress determined via $R(\delta)$.

Analyses of the plastic energy expended to the end of failure are shown in Fig. 21 as a function of $\log(V_i)$, also Fig. 13 in the Appendix. The numerical results approach relatively well the experimental results shown in Fig. 12. At lower imposed velocities the standard and U-geometry show a positive rate sensitivity for both experiment and numerics with maximum values of the energies slightly lower than found in experiment. However, in experiment the total energy to failure was determined.

In both cases, numerics and experiment, a drop in energy is observed at high velocities, with the lowest level ~3 J. In the case of sharp stress concentrators the level of energy is low also at low impact velocities, for numerics ~2 J to 4 J and for experiment ~6 J for the V and sharp notches. On the contrary to the experiment the V-notch shows an increase of the plastic energy at high imposed velocities, due to the transition mechanism discussed earlier. Perhaps some geometrical and experimental imperfections eliminated this transition during experiments.

9. Discussion and conclusions

The experimental and numerical study of adiabatic stress concentrators performed for VAR 4340 steel, ~50 HRC, have demonstrated a strong effect of the imposed velocity on failure development in every geometry studied. At higher impact velocities a substantial decrease of energy to fracture for VAR 4340 steel was revealed. At impact velocities around 120 m/s existence of the CIV in shear has been confirmed, [1, 5, 9], both by experiments and numerics.

Relatively high increase of the local temperatures around the notch concentrators promotes, to some extent, a local development of the ASB's. The ASB's can propagate

later with a high speed. In fact, formation of ASB is a kind of fracture mechanism. A more detailed discussion of this subject can be found elsewhere, [15].

Introduction to FE code the failure criterion based on the instability strain in plastic shearing has enabled to calculate fracture processes under impact. It has been shown that this local failure criterion is sensitive to the local strain rate. The other possible criterion of the adiabatic failure can be founded on the « strain energy density » concept. Also in this case the criterion depends on the local strain rate. Both criteria lead to similar results in numerical calculations. However, 3D cases should be analyses further, including the type of element used in FE codes. The preliminary numerical analyses with the local failure criterion confirmed experimental findings, especially the reduction of failure energies at high imposed velocities. The approach presented in this Project can be applied in numerical studies of more complex fragmentation processes in steels.

REFERENCES

[1] J.R.Klepaczko, Experimental Investigation of Adiabatic Shear Banding at Different Impact Velocities, Final Technical Report for the ERO of the US Army, Contract N° DAJA45-90-C-0052, LPMM-Metz, (1993).

[2] J.R.Klepaczko, P.Lipinski and A.Molinari, An analysis of the thermoplastic catastrophic shear in some metals, in: Impact Loading and Dynamic Behavior of Materials, DGM Informationsgesellschaft Verlag, Oberursel, Vol. 2, (1988), 69.

[3] J.R.Klepaczko and B.Rezaig, A numerical study of adiabatic shear banding in mild steel by dislocation mechanics based constitutive relations, Mech. of Materials, **24** (1996), 125.

[4] A.Marchand and J.Duffy, An experimental study of the formation process of adiabatic shear bands in a structural steel, J. Mech. Phys. Solids, **36**, 251, (1988).

[5] M.Klósak and J.R.Klepaczko, Numerical Study of the Critical Impact Velocity in Shear, Appendix N°1 to the Final Technical Report, Contract N68171-95-C-9071, LPMM-Metz, France (1996).

[6] M.Klósak and J.R.Klepaczko, Numerical study of the inelastic wave propagation and plastic instabilities with thermal coupling, Proc. 13th Polish Conference on Computer Methods in Mechanics, Poznan, Poland, Vol. II, (1997), 615.

[7] J.R.Klepaczko, An experimental technique for shear testing at high and very high strain rates. The case of mild steel, Int. J. Impact. Engng., **15** (1994), 25.

[8] J.R.Klepaczko, Plastic shearing at high and very high strain rates, Proc. Conf. EURODYMAT 94, J. de Phys., IV, Coll. C8, (1994), C8-35.

[9] J.R.Klepaczko, Recent progress in testing of materials in impact shearing, in: Dynamic Fracture, Failure and Deformation, PVP-Vol. 300, ASME, NY (1995), 165.

[10] J.R.Klepaczko, On the critical impact velocity in plastic shearing, EXPLOMET'95, Proc. Int. Conf. On Metallurgical and Materials Applications of Shock Waves and High Strain Rate phenomena, Elsevier Science, Amsterdam, (1995), 147.

[11] N.Cristescu, Dynamic Plasticity, North-Holland Publ. Co., Amsterdam, (1967).

[12] Th.Kàrmàn and P.Duwez, The propagation of plastic deformation in solids, J. of Appl. Phys., **21**, (1950), p.987.

[13] J.R.Klepaczko, Generalized conditions for stability in tension tests, Int. J. Mech. Sci., **10**, (1968), 297.

[14] F.H.Wu and L.B.Freund, Deformation trapping due to thermoplastic instability in one dimensional wave propagation, J. Mech. Phys. Solids, **32**, (1984), 119.

[15] Stress Concentrators and Rate Effects in Formation of Adiabatic Shear Bands, Final Technical Report, Contract N° N68171-95-C-9071, LPMM-Metz, (1996).

[16] J.R.Klepaczko, A practical stress-strain rate-rate temperature constitutive relation of the power form, J. Mech. Working Technology, **15**, (1987), 143.

[17] J.R.Klepaczko, Modeling of Structural evolution at medium and high strain rates, FCC and BCC metals, in: Constitutive relations and Their Physical Basis, Proc. 8th Risö Mater. Symp., Risö Natl. Lab. (1987), 387.

[18] M.B.Bever, D.L.Holt and A.L.Titchener, The stored energy of cold work, in Progress in Material Science, Vol. 17, Pergamon Press, Oxford (1973).

[19] J.R.Klepaczko, Dynamic crack initiation, some experimental methods and modeling, in: Crack Dynamics in Metallic Materials, Springer Verlag, Vienna (1990).

[20] I.V.Varfolomeyev and J.R.Klepaczko, Approximate Analysis on Strain Rate Effects and Behavior of Stress and Strain Fields at the Crack Tip in Mode II in Metallic Materials, Appendix N°1 To the Technical Report ERO US Army RDSG, Contract DAJA 45-90-C-0052 (1992).

[21] I.V.Varfolomeyev and J.R.Klepaczko, Effect of strain rate on the geometry of the plastic zone near a Mode II crack tip, parametrical analysis, Strength of Materials (Problems Prochnosti), English translation, N°3, **27** (1995), 138.

[22] M.Zhou, A.J.Rosakis and G.Ravichandran, Dynamically Propagating Shear Bands in Impact-Loaded Prenotched Plates, SM Report 94-01, California Inst. of Technology, Pasadena, CA (1995).

FIGURE CAPTIONS

Fig. 1 Configuration of experimental setup for impact shearing of the MDS specimen.

Fig. 2 Oscillogram of the test on MDS specimen, VAR 4340 steel (standard geometry), loaded by projectile L_p=200 mm with impact velocity 72.3 m/s.

Fig. 3 Nominal shear strains of instability Γ_{nc} and Γ_{nl} as a function of impact velocity V_i.

Fig. 4 Fracture energy versus impact velocity V_i.

Fig. 5 Schematic stress-strain curve showing different stages of fast (adiabatic) shearing.

Fig. 6 Scheme of an adiabatic stress concentrator charged by approaching elastic-plastic shear wave (shadowed bar) excited by shear velocity V_0.

Fig. 7 Specimen geometries with different stress concentrators.

Fig. 8 Strain rate spectrum for the mean values of τ_m, VAR 4340 steel, ~50 HRC, four geometries.

Fig. 9 Strain rate spectrum for the mean values of τ_c, VAR 4340 steel, ~50 HRC, four geometries.

Fig. 10 Strain rate spectrum for the mean values of Γ_m, VAR 4340 steel, ~50 HRC, four geometries.

Fig. 11 Strain rate spectrum for the mean values of Γ_c, VAR 4340 steel, ~50 HRC, four geometries.

Fig. 12 Strain rate spectrum for the mean energy of failure, VAR 4340 steel, ~50 HRC, four geometries.

Fig. 13 Schematic evolution of stress-strain curves of industrial steels at strain rates higher than $5 \cdot 10^2$ 1/s; (1) ~$5 \cdot 10^2$ 1/s; (2) ~$5 \cdot 10^3$ 1/s; (3) ~$1 \cdot 10^4$ 1/s; (4) ~$5 \cdot 10^4$ 1/s;

Fig. 14 Local failure criteria applied in FE calculations, critical shear strain and critical energy density.

Fig. 15 Final stages of failure in deformed configuration for standard geometry loaded by three incident velocities V_i, plane B is the support side.

Fig. 16 Final stages of failure in deformed configuration for U-geometry loaded by three incident velocities V_i, plane B is the support side.

Fig. 17 Final stages of failure in deformed configuration for V-geometry loaded by three incident velocities V_i, plane B is the support side.

Fig. 18 Final stages of failure in deformed configuration for sharp-notch geometry loaded by three incident velocities V_i, plane B is the support side.

Fig. 19 Four patterns of failure for V-geometry loaded at different incident velocities.

Fig. 20 Maximum reaction force as a function of impact velocity; four types of specimen geometry; logarithmic scale of imposed velocity.

Fig. 21 Dissipated plastic energy versus imposed velocity; four geometries.

LIST OF PUBLICATIONS ASSOCIATED WITH THE LAST YEAR OF THE CONTRACT (1996/1997)

[1] M.Klósak and J.R.Klepaczko, Numerical study of the inelastic wave propagation and plastic instabilities with thermal coupling, Proc. 13th Polish Conference on Computer Methods in Mechanics, Poznan, Poland, Vol. II, (1997), 615.

[2] J.R.Klepaczko and M.Klósak, Numerical study of the Critical Impact Velocity in shear, European J. of Mech., A/Solids, (1998), submitted.

[3] J.R.Klepaczko, Remarks on impact shearing, J. Mech. Phys. Solids, **45** (1998), in print.

[4] J.R.Klepaczko, M.Klósak and T.Lodygowski, Dynamic Instabilities in high-speed shearing, Proc. ABAQUS Users' Conference, Newport, RI, (1998), submitted.

[5] J.R.Klepaczko, Adiabatic stress concentrators in impact shearing, Int. J. Impact Engng., in preparation.

FIGURES FROM 1 TO 21

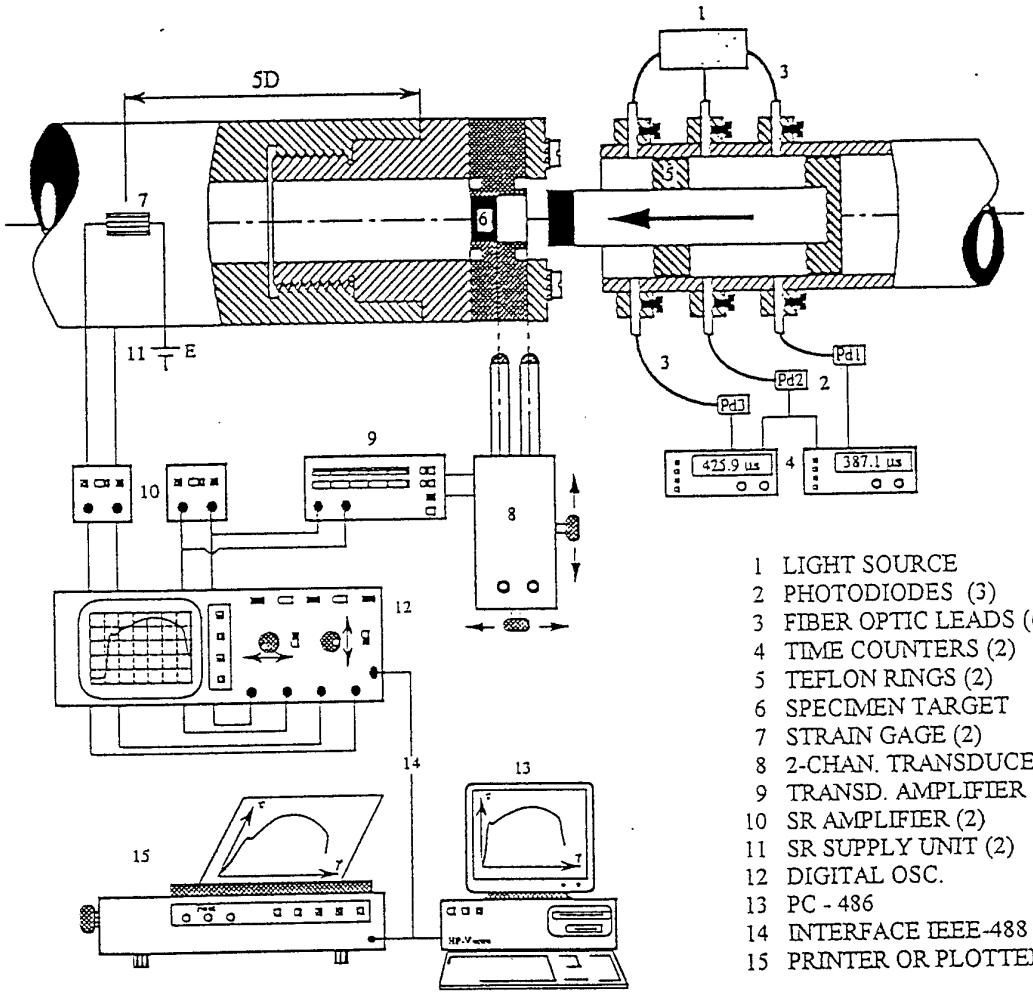

1 LIGHT SOURCE
2 PHOTODIODES (3)
3 FIBER OPTIC LEADS (6)
4 TIME COUNTERS (2)
5 TEFLON RINGS (2)
6 SPECIMEN TARGET
7 STRAIN GAGE (2)
8 2-CHAN. TRANSDUCER
9 TRANSD. AMPLIFIER
10 SR AMPLIFIER (2)
11 SR SUPPLY UNIT (2)
12 DIGITAL OSC.
13 PC - 486
14 INTERFACE IEEE-488
15 PRINTER OR PLOTTER

Fig. 1

FILES: 17DV3.NGF

```
*CLS
    *IDN?
        HEWLETT-PACKARD,54510A,3022A01063,0123
                                        :PRINT?
```

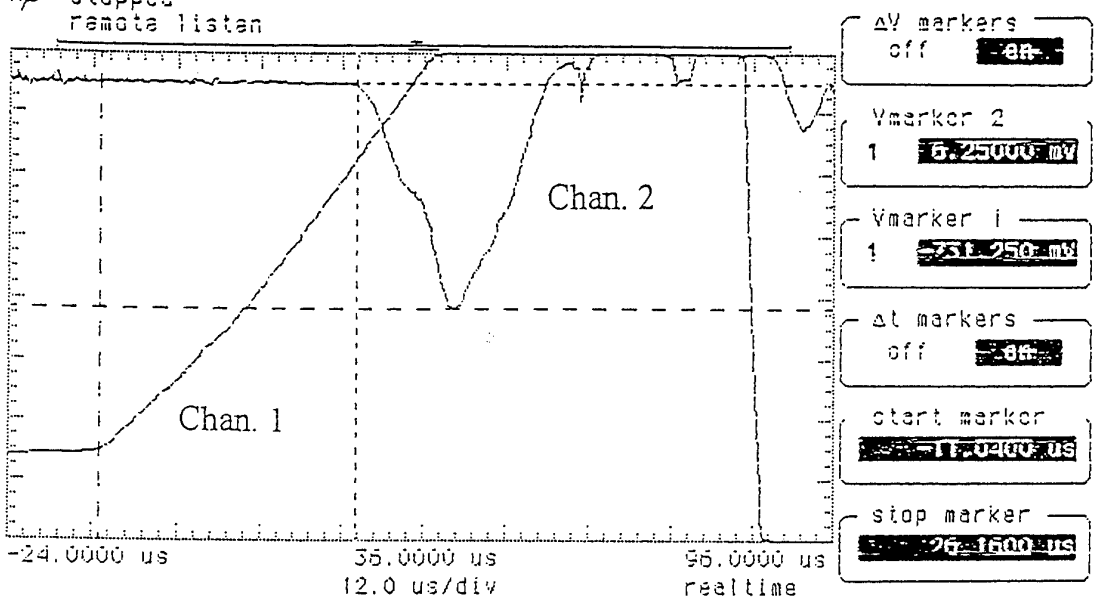


```
 Vmarker2( 1 )   -6.25000mV      stop marker:   26.1600us
 Vmarker1( 1 )   -731.250mV     start marker:  -11.0400us
   delta V( 1 )   725.000mV         delta t:    37.2000us
                                 1/delta t:    26.8817kHz                fine

              Sensitivity    Offset          Probe       Coupling   Impedance
Channel 1     200  mV/div  -700.000 mV       1:1           dc        1M ohm
Channel 2     999  mV/div  -1.99800  V    0.999:1          dc        1M ohm

  Trigger Mode: Edge
On the Positive Edge of Channel2
Trigger Level(s)
  Channel2 = -3.74625  V (noise reject ON)
HoldOff = 700.000 ns
```

Fig. 2

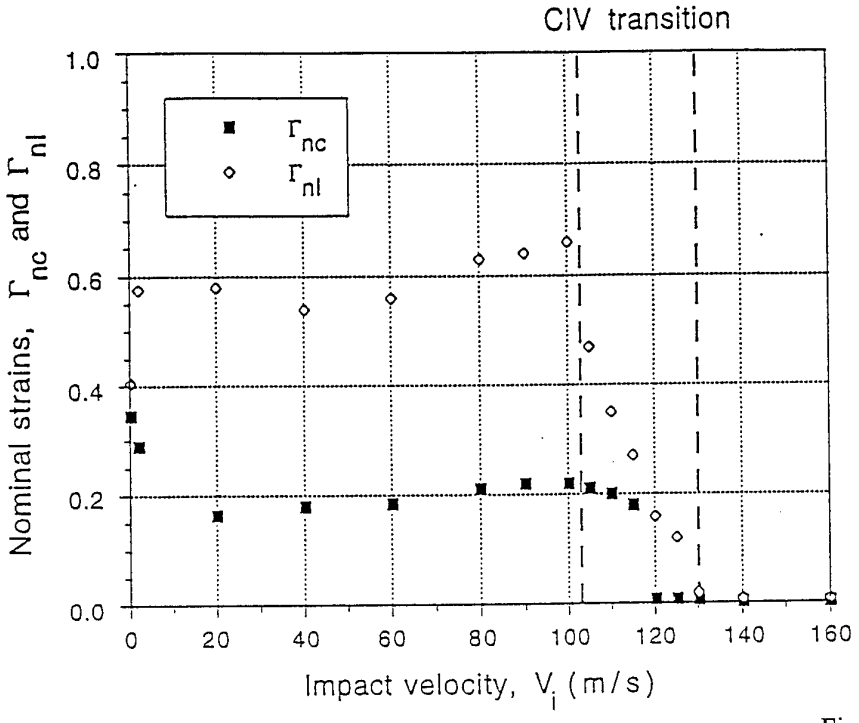
CIV transition
Nominal strains, Γ_{nc} and Γ_{nl}
Γ_{nc}
Γ_{nl}
1.0
0.8
0.6
0.4
0.2
0.0
0
20
40
60
80
100
120
140
160
Impact velocity, V_i (m/s)

Fig. 3

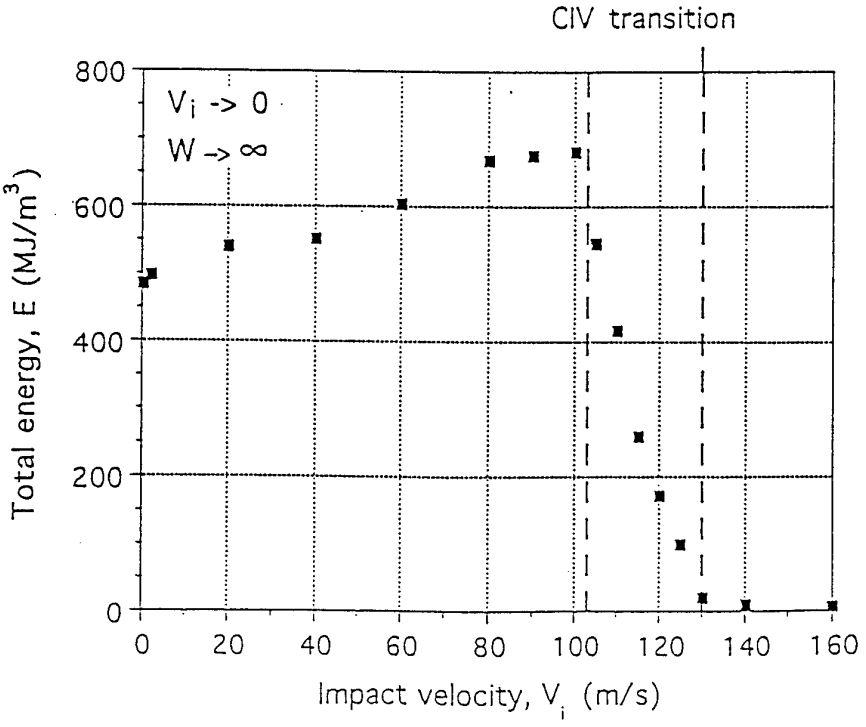
CIV transition
V_i -> 0
W -> ∞
Total energy, E (MJ/m^3)
800
600
400
200
0
0
20
40
60
80
100
120
140
160
Impact velocity, V_i (m/s)

Fig. 4

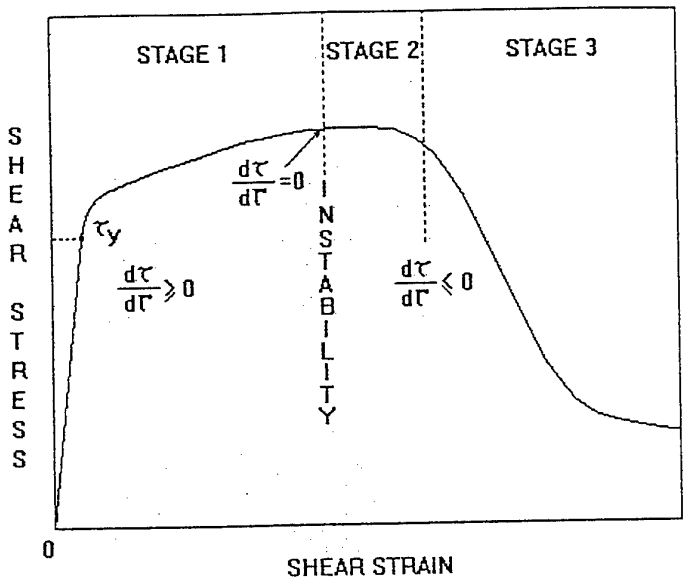
STAGE 1
STAGE 2
STAGE 3
SHEAR STRESS
$\frac{d\tau}{d\Gamma}=0$
τ_y
$\frac{d\tau}{d\Gamma}\geqslant 0$
INSTABILITY
$\frac{d\tau}{d\Gamma}\leqslant 0$
0
SHEAR STRAIN

Fig. 5

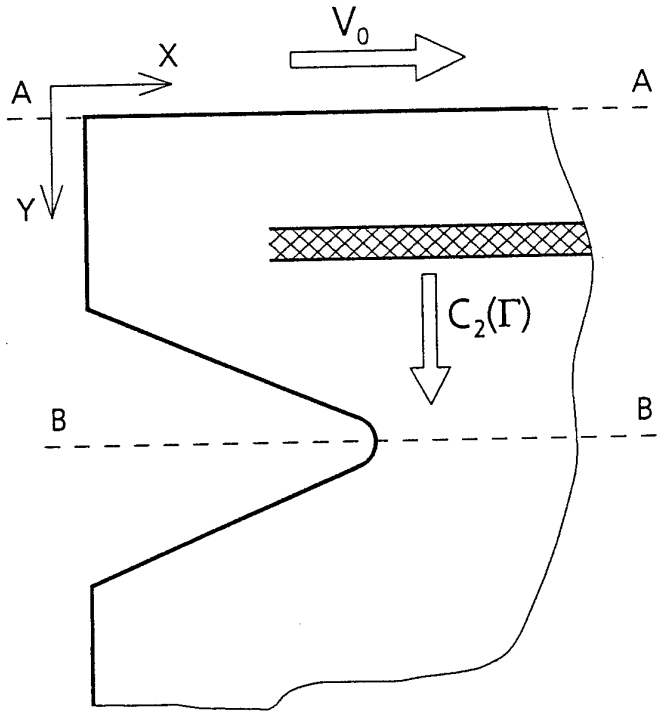
V_0
X
A
A
Y
$C_2(\Gamma)$
B
B

Fig. 6

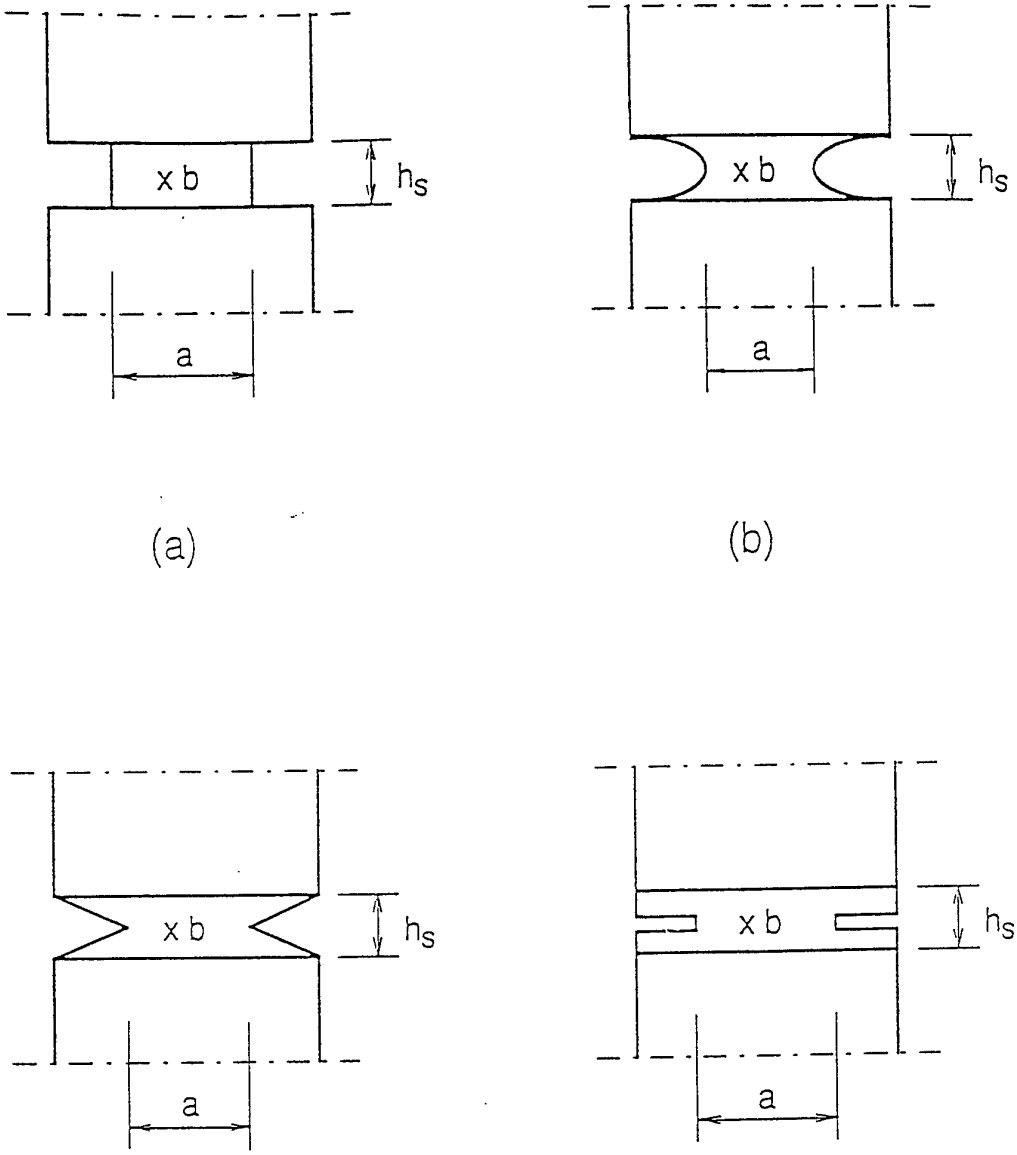

Fig. 7

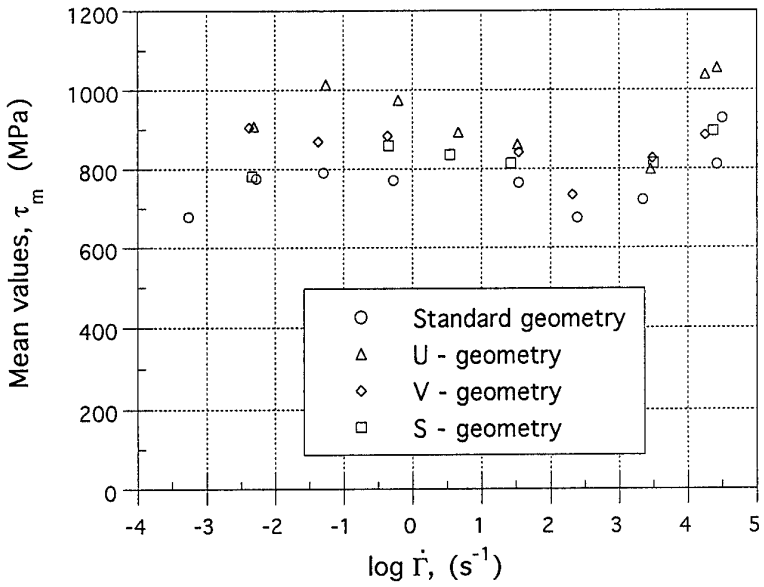
1200
1000
800
600
400
200
0
-4
-3
-2
-1
0
1
2
3
4
5
Mean values, τ_m (MPa)
log $\dot{\Gamma}$, (s^{-1})
Standard geometry
U - geometry
V - geometry
S - geometry

Fig. 8

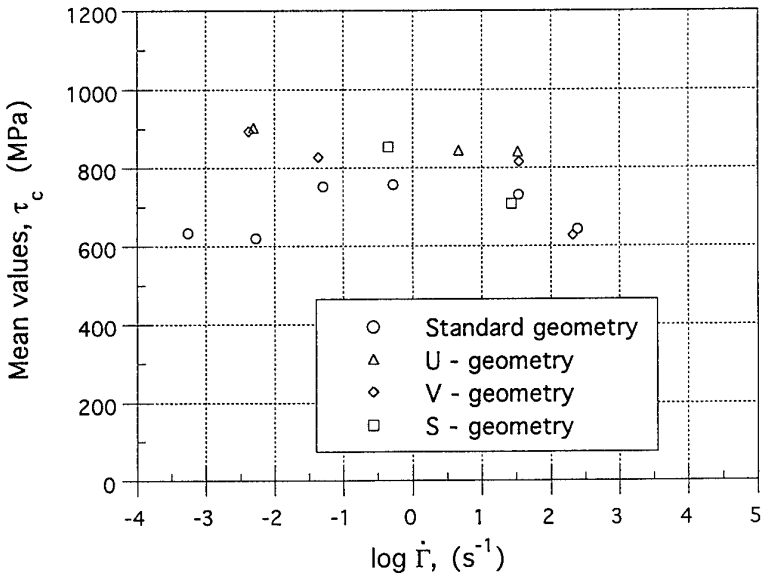
1200
1000
800
600
400
200
0
-4
-3
-2
-1
0
1
2
3
4
5
Mean values, τ_c (MPa)
log $\dot{\Gamma}$, (s^{-1})
Standard geometry
U - geometry
V - geometry
S - geometry

Fig. 9

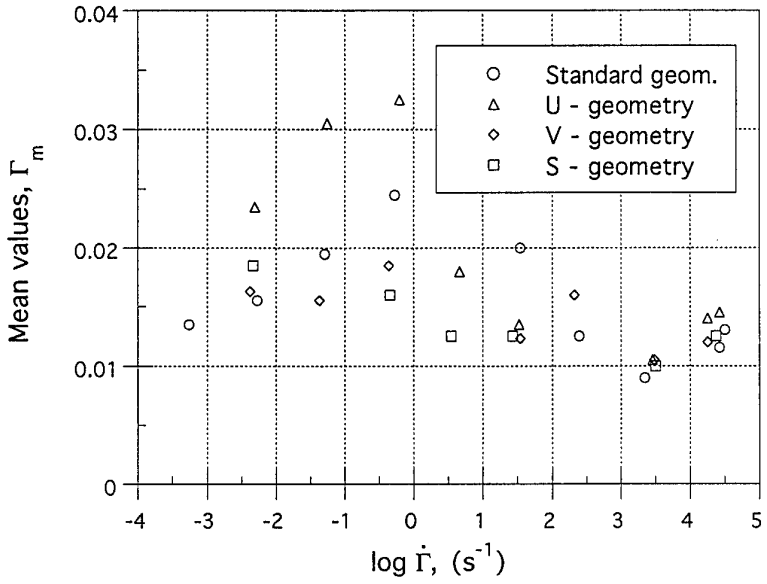
0.04
0.03
0.02
0.01
0
Mean values, Γ_m
-4
-3
-2
-1
0
1
2
3
4
5
log $\dot{\Gamma}$, (s^{-1})
Standard geom.
U - geometry
V - geometry
S - geometry

Fig. 10

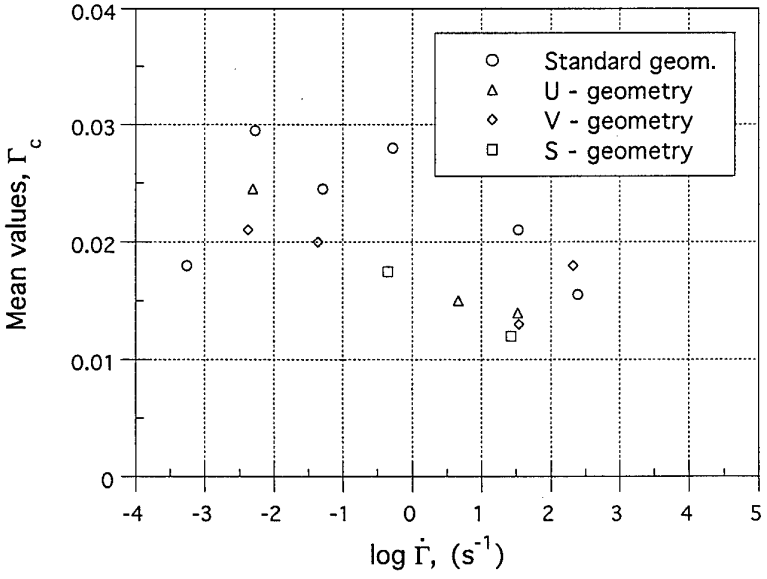
0.04
0.03
0.02
0.01
0
Mean values, Γ_c
-4
-3
-2
-1
0
1
2
3
4
5
log $\dot{\Gamma}$, (s^{-1})
Standard geom.
U - geometry
V - geometry
S - geometry

Fig. 11

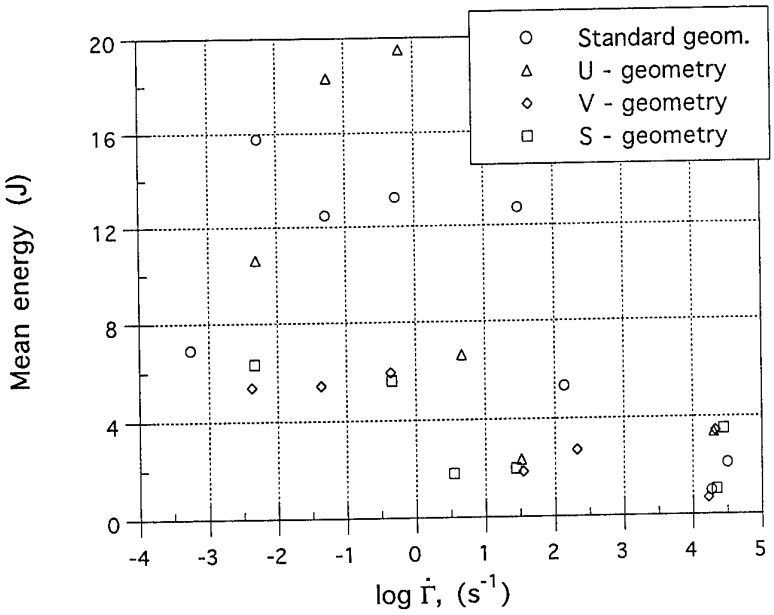
Standard geom.
U - geometry
V - geometry
S - geometry
Mean energy (J)
20
16
12
8
4
0
-4
-3
-2
-1
0
1
2
3
4
5
log Γ̇, (s^{-1})

Fig. 12

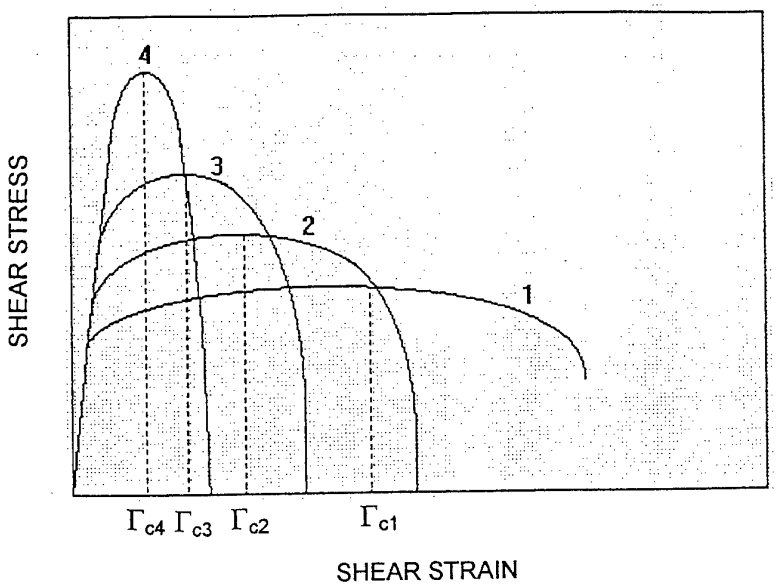
4
3
2
1
SHEAR STRESS
Γc4 Γc3 Γc2 Γc1
SHEAR STRAIN

Fig. 13

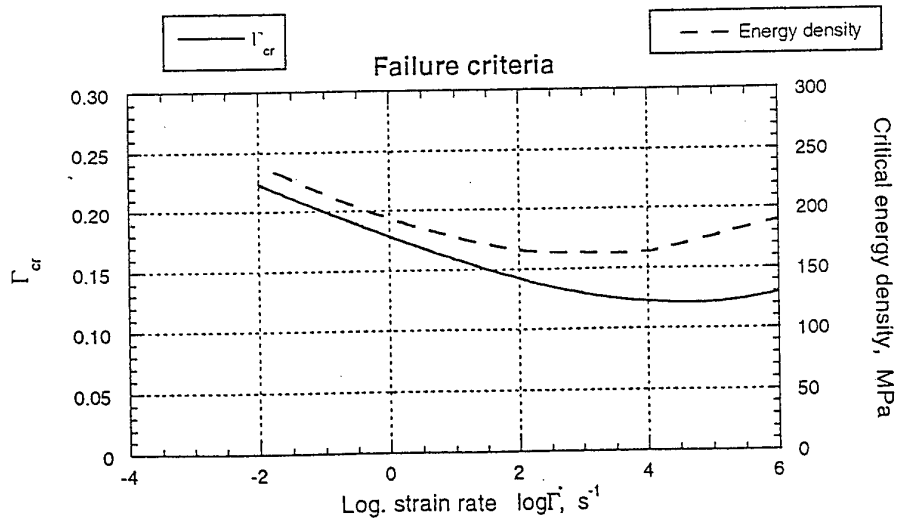
Γ̇cr
Energy density
Failure criteria
0.30
0.25
0.20
0.15
0.10
0.05
0
Γcr
300
250
200
150
100
50
0
Critical energy density, MPa
-4
-2
0
2
4
6
Log. strain rate logΓ̇, s-1

Fig. 14

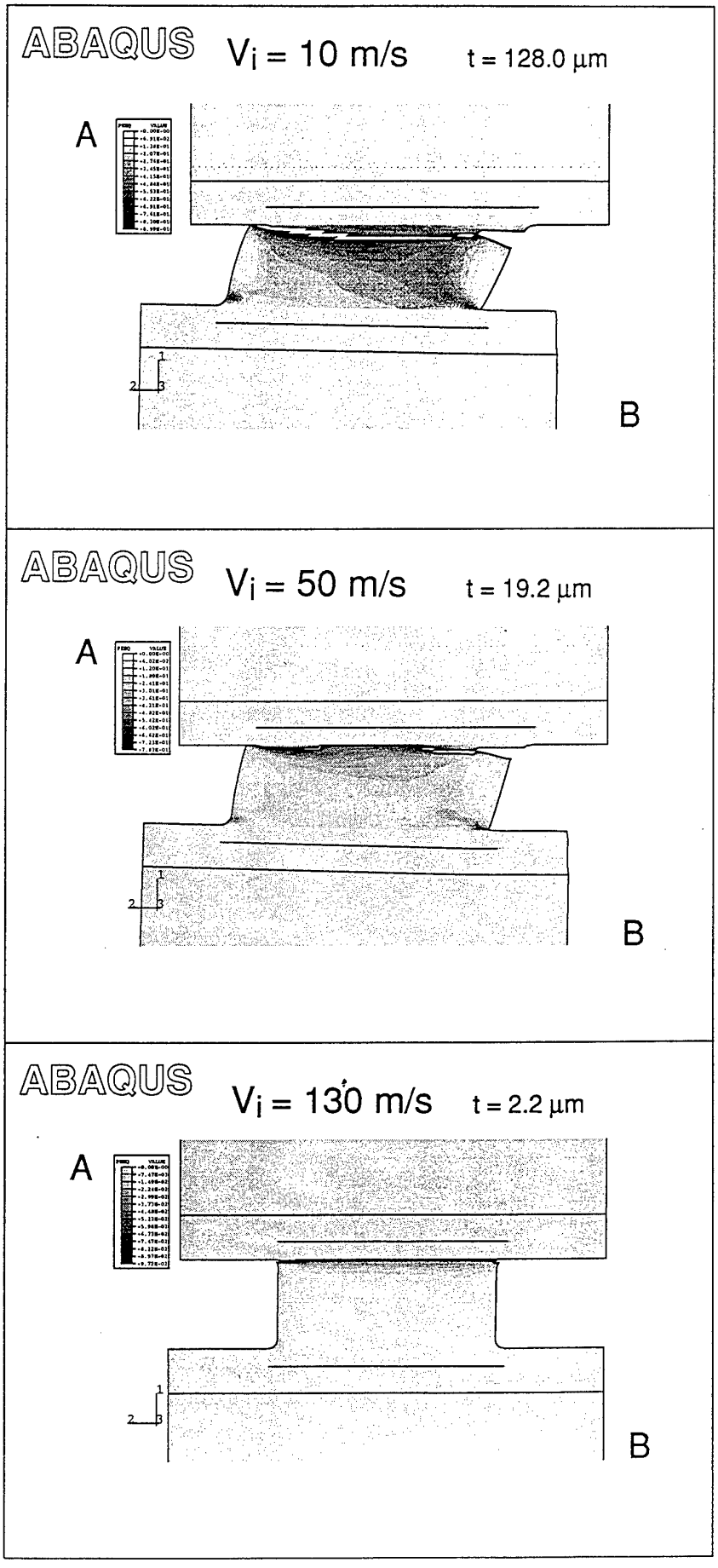
ABAQUS
V_i = 10 m/s
t = 128.0 μm
A
B
ABAQUS
V_i = 50 m/s
t = 19.2 μm
A
B
ABAQUS
V_i = 130 m/s
t = 2.2 μm
A
B

Fig. 15

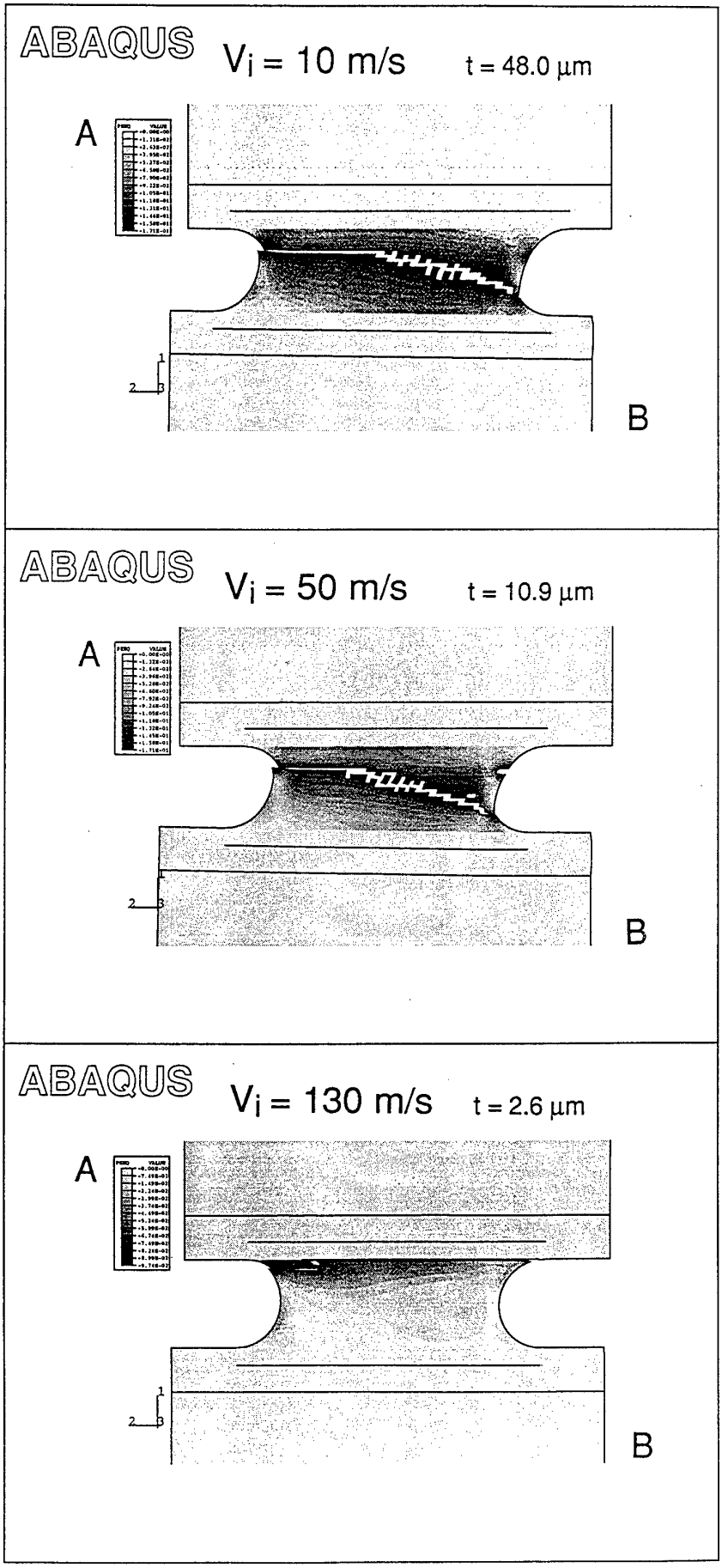
ABAQUS
V_i = 10 m/s
t = 48.0 μm
A
B
ABAQUS
V_i = 50 m/s
t = 10.9 μm
A
B
ABAQUS
V_i = 130 m/s
t = 2.6 μm
A
B

Fig. 16

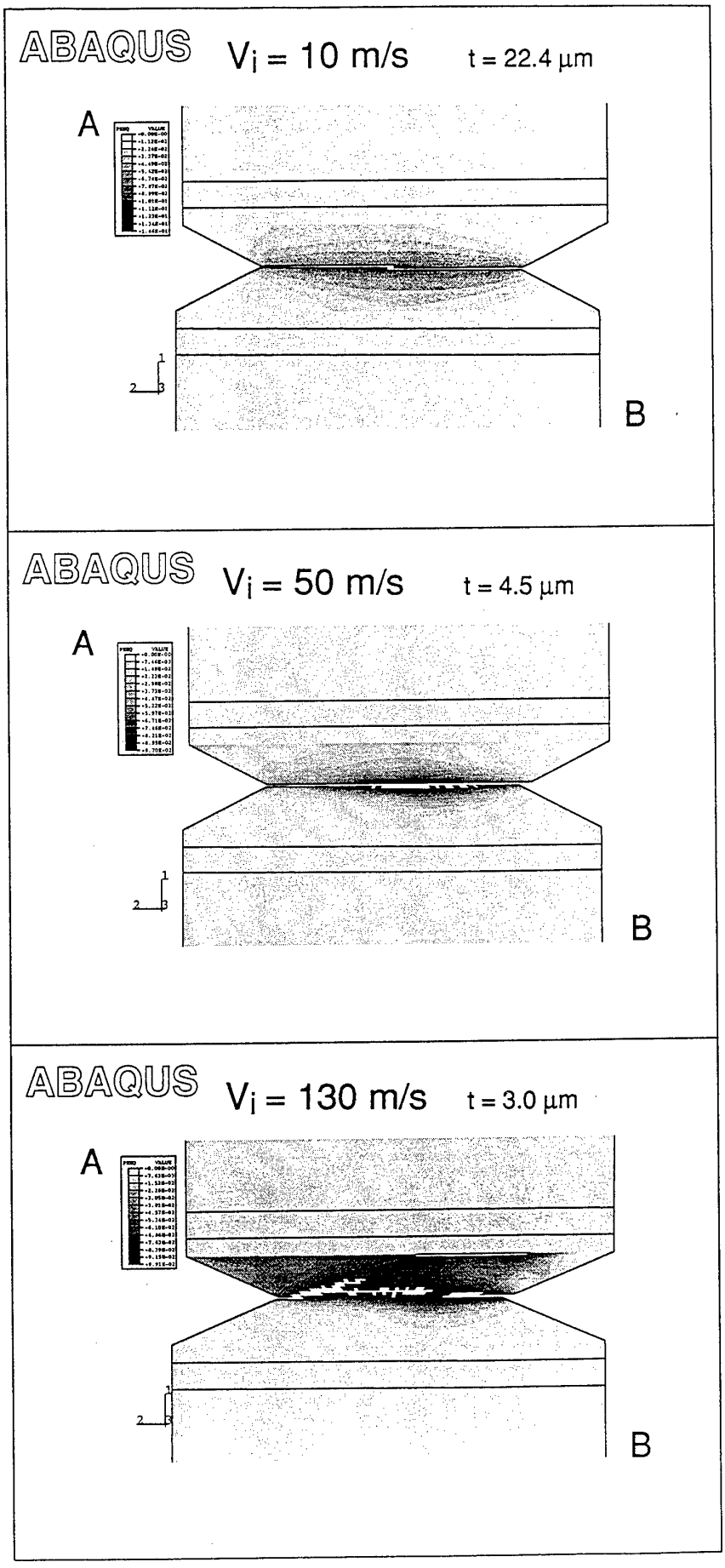
ABAQUS
V_i = 10 m/s
t = 22.4 μm
A
B
ABAQUS
V_i = 50 m/s
t = 4.5 μm
A
B
ABAQUS
V_i = 130 m/s
t = 3.0 μm
A
B

Fig. 17

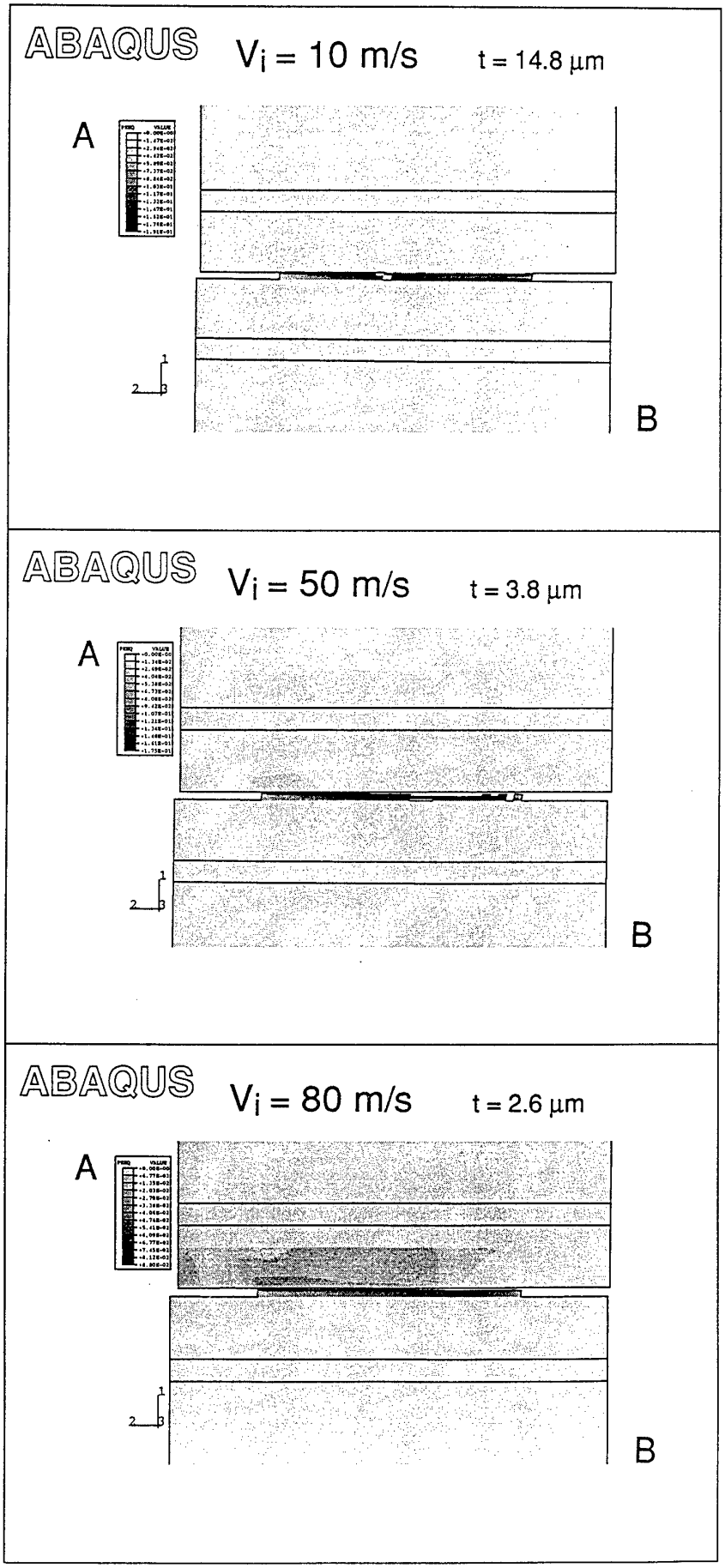
ABAQUS
V_i = 10 m/s
t = 14.8 μm
A
B
ABAQUS
V_i = 50 m/s
t = 3.8 μm
A
B
ABAQUS
V_i = 80 m/s
t = 2.6 μm
A
B

Fig. 18

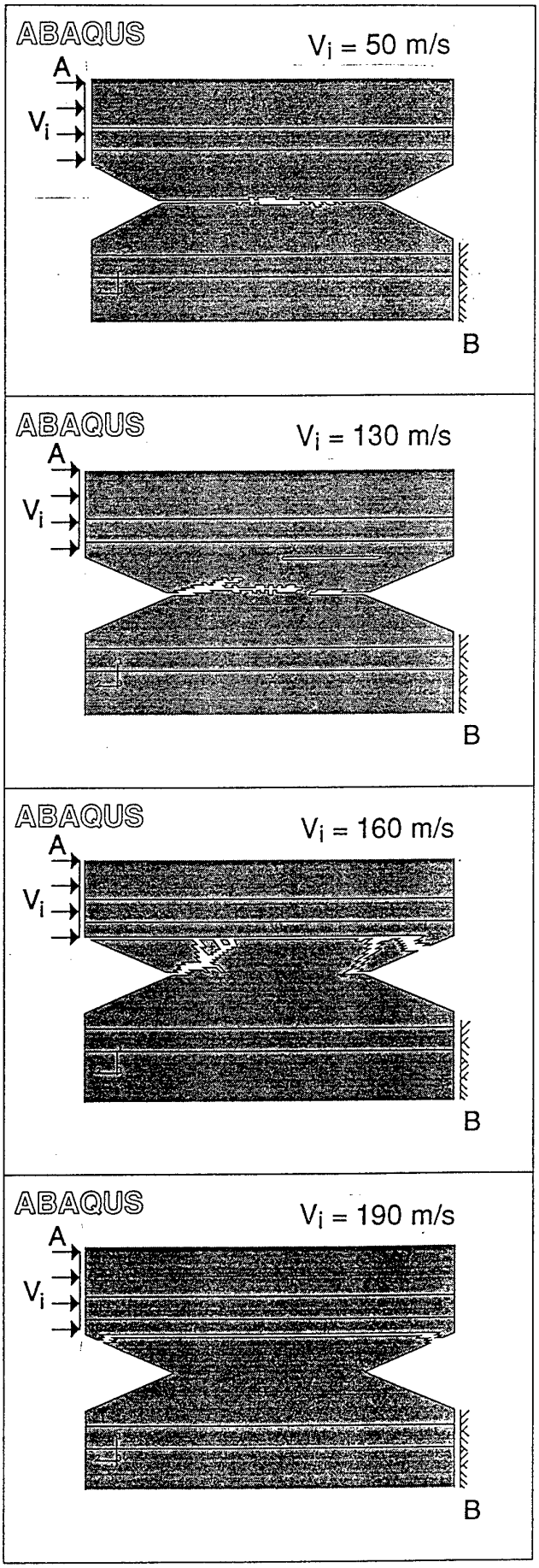
ABAQUS
V_i = 50 m/s
A
V_i
B
ABAQUS
V_i = 130 m/s
A
V_i
B
ABAQUS
V_i = 160 m/s
A
V_i
B
ABAQUS
V_i = 190 m/s
A
V_i
B

Fig. 19

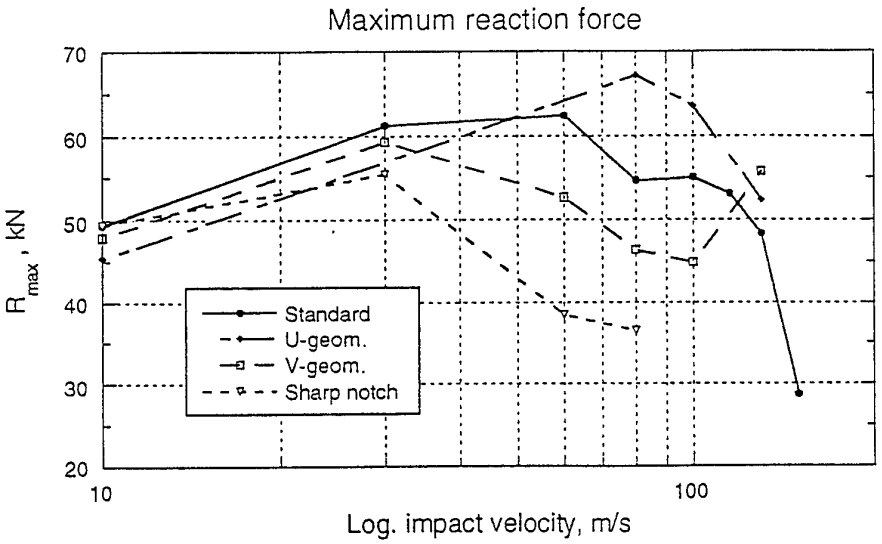
Maximum reaction force
70
60
50
40
30
20
10
100
R_{max}, kN
Log. impact velocity, m/s
Standard
U-geom.
V-geom.
Sharp notch

Fig. 20

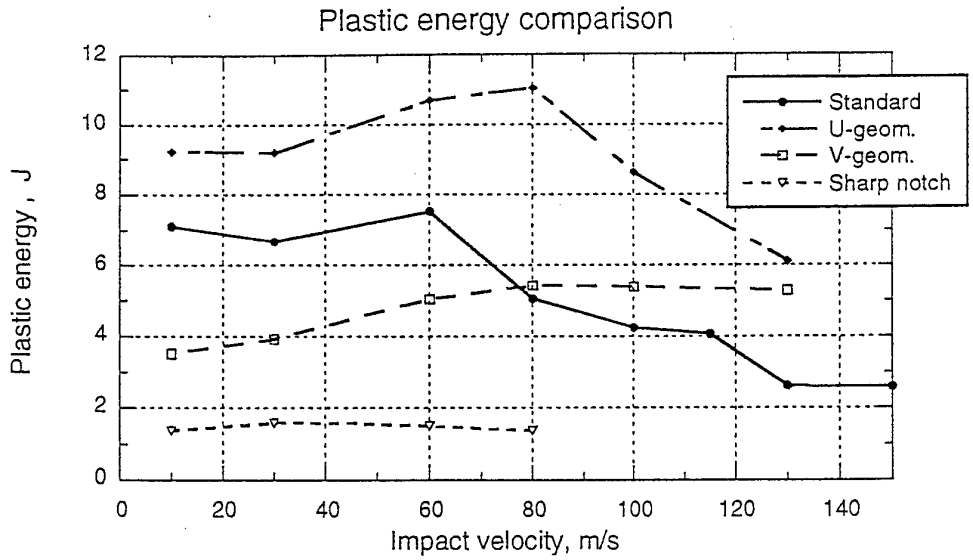
Plastic energy comparison
12
10
8
6
4
2
0
0
20
40
60
80
100
120
140
Plastic energy, J
Impact velocity, m/s
Standard
U-geom.
V-geom.
Sharp notch

Fig. 21